

# Overview of Resistive Random Access Memory (RRAM): Materials, Filament Mechanisms, Performance Optimization, and Prospects

Hong Wang and Xiaobing Yan\*

Because conventional nonvolatile memory is limited by process technology and physical size, resistive random access memory (RRAM) gradually enters the field of view due to its simple structure, fast program/erase speed, low power consumption, and so on. This review article summarizes the materials, filament mechanisms, performance optimization, and application prospects of RRAM structures to provide readers with a reference for future investigation. The filament mechanisms, which involve the electrochemical metallization mechanism (ECM), valence change mechanism (VCM), and thermochemical mechanism (TCM), of RRAM devices are particularly highlighted. The parameters that determine the RRAM characteristics such as operating voltages, ON/OFF ratio, endurance, and data retention are improved by incorporating the three methods: 1) “interface engineering”, 2) element doping of functional materials, and 3) introduction of low-dimensional materials. In the last section, a brief introduction to the future RRAM application prospects and challenges is provided.

## 1. Introduction


In biological neuromorphic systems, information transmission between two neurons is inseparable from synapses.<sup>[1]</sup> With the development of artificial intelligence, artificial synapses have become the focus of research for scientists. Researchers have attempted to enable the main memory functional devices of modern computers to simulate biological synaptic functions.<sup>[2–4]</sup> Memory can be divided into volatile memory and nonvolatile memory, which can realize the long-term storage of digital information and provide an effective medium for the inheritance and development of human civilization. Currently, silicon-based flash memory dominates the data storage market.<sup>[5–7]</sup> With the

miniaturization of electronic products, there is a high demand for small-sized, high-performance, low-voltage, and low-power storage devices.<sup>[8,9]</sup> However, flash memory with a high operating voltage and low retention capacity has reached its physical and technological limit that cannot meet the needs of storage devices in the future.<sup>[10,11]</sup> As early as 1967, Simmons and Verderber reported resistance switching in Au/SiO<sub>2</sub>/Al resistive random access memory (RRAM) devices consisting of two electrode layers and an intermediate functional layer.<sup>[12]</sup> It is a new type of memory device with a simple sandwiched structure, as shown in Figure 1a,b.<sup>[13–15]</sup> Resistive switching devices can achieve the storage of “0” or “1” by utilizing the low/high resistance (ON/OFF state) transformation of the functional materials. Figure 1c,d illustrates

typical bipolar/unipolar  $I$ – $V$  characteristic curves of a resistance change memory. When a cyclic scanning voltage is applied to the device, it transits from a high-resistance state to a low-resistance state (SET) or vice versa (RESET). Compared to traditional flash memories, RRAM devices with low operating voltage, low power consumption, high speed, and high density are more noteworthy.<sup>[16,17]</sup> Moreover, the fabrication process of RRAMs is compatible with the traditional complementary metal oxide semiconductor (CMOS) process, which is conducive to the advancement of scientific research. However, there are still some unresolved challenges in terms of resistive switching materials, device stability, parameter dispersion, and storage mechanisms.<sup>[18]</sup> With the in-depth study of resistive switching memory, RRAM devices are being gradually used to mimic the biosynaptic function for providing a direction in the field of electronic artificial synapse.<sup>[2–4]</sup>

In this article, we review recent research and focus on the following four aspects of RRAM: materials, filament mechanisms, performance optimization, and application prospects. First, we systematically combed through the resistive switching materials used in the past and recent years, because materials play a key role in device performance. At present, low-dimensional material devices are the main research hotspot; however, their performance reliability and their large-area growth process technology are still difficult problems to be solved in the future. Second, although filament mechanisms confirmed by many researchers have been introduced, the resistance switching mechanism of RRAM devices is still controversial in the academic world

Dr. H. Wang, Prof. X. Yan  
Key Laboratory of Digital Medical Engineering of Hebei Province  
Key Laboratory of Optoelectronic Information Materials of Hebei Province  
College of Electron and Information Engineering  
Hebei University  
Baoding 071002, P. R. China  
E-mail: yanxiaobing@ime.ac.cn, xiaobing\_yan@126.com  
Prof. X. Yan  
Department of Materials Science and Engineering  
National University of Singapore  
Singapore 117576, Singapore

 The ORCID identification number(s) for the author(s) of this article can be found under <https://doi.org/10.1002/pssr.201900073>.

DOI: 10.1002/pssr.201900073

and there is no consensus. The most important aspect is that a device with superior performance is the ultimate goal of the research; therefore, the discussion of three methods to improve the performance of the device, presented here, is mainly aimed at providing readers with a reference for future investigation. In general, the small, low-power, and environment-friendly RRAM devices will be the main direction of future development. Finally, the application prospects of the resistive memory and the current challenges are briefly introduced.

## 2. Materials for RRAM

Many materials have been found to exhibit resistance change properties under electrical field or current stimulus. The storage mediums for RRAM can be divided into two categories: organic materials and inorganic materials, as shown in **Figure 2**. Organic materials, which mainly involve the bioinspired organic materials (such as silk fibroin,<sup>[19,20]</sup> albumen,<sup>[21]</sup> nanocellulose,<sup>[22]</sup> and bovine serum albumin<sup>[23]</sup>) and polymer organic materials (such as “PVPCz59”, i.e. PVPCz (poly(9-(4-vinyl phenyl) carbazole): P2VP (poly(2-vinyl pyridine)) = 59:41,<sup>[24]</sup> “PVDR” (nanoaggregated dispersed red 1-grafted poly(*N*-vinylcarbazole)),<sup>[25]</sup> “PVK-C<sub>60</sub>” (poly(*N*-vinylcarbazole) with covalently attached fullerene (C<sub>60</sub>)),<sup>[26]</sup> and other materials<sup>[27–33]</sup>), have attracted the attention of many researchers for application in flexible/wearable memristive devices and single-use monitoring devices for health diagnosis. However, the stability of organic materials, which leads to high SET/RESET voltage, power consumption, and dispersed voltage distribution characteristics of RRAM devices, needs to be further strengthened, and the supply of materials is also a problem that needs to be resolved.<sup>[19–22,28–37]</sup> On the other hand, inorganic materials can be manufactured by simple processes, show stable performance, have low cost, and are receiving extensive attention from researchers. We mainly introduce solid electrolyte, oxides, and low-dimension system of the inorganic resistive switching materials.<sup>[38–61]</sup> Binary oxides have attracted attention in the electronics field due to their simple structure, ease of control in material composition, low cost, and compatibility with conventional processes. For example, as early as the 1960s,

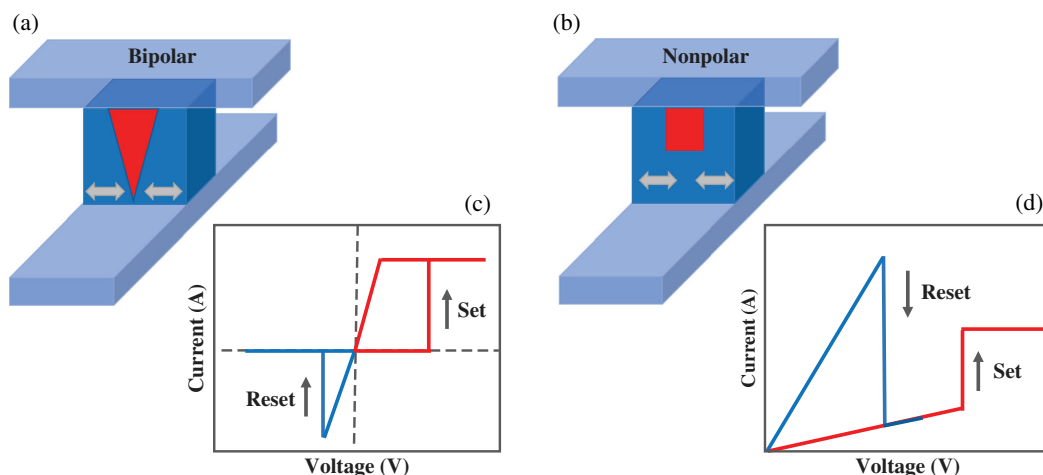


**Hong Wang** received the MS degree from Hebei University, Baoding, China, in 2018. She is currently pursuing a PhD degree in Department of Physics at Hebei University, Baoding, China. Her research interest includes the design and application of 2D material-based memory devices.

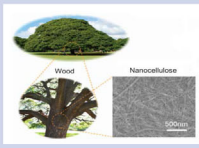

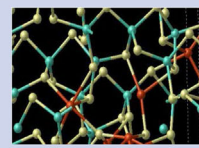
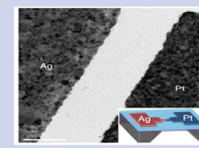
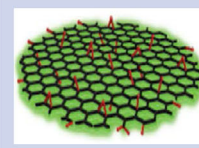
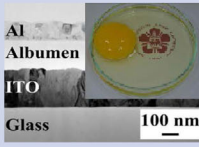

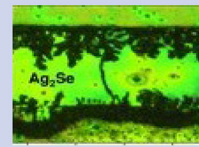
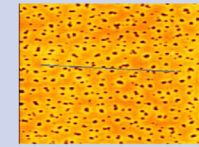
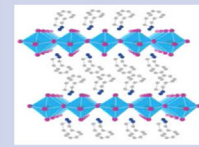

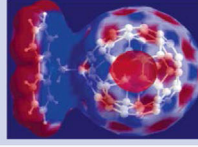
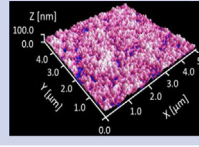
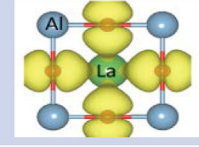
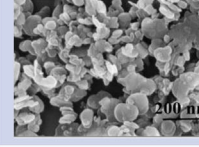


**Xiaobing Yan** received his PhD degree from Nanjing University, Nanjing, China, in 2011. He is currently a Professor with the College of Electron Information and Engineering, Hebei University, Baoding, China. His current research interests include the study of emerging memories, such as charge trapping memory, phase change memory, resistive switching memory, and brain-inspired neuromorphic devices.

the Hickmott's research group in the United States reported the current-voltage curve in the Al/Al<sub>2</sub>O<sub>3</sub>/Al device structure, which has a resistive switching characteristic, under the action of an electric field.<sup>[38]</sup> Thereafter, TiO<sub>2</sub><sup>[39]</sup> materials were introduced that could reduce the memory switching voltage and achieve good endurance characteristics over 10<sup>4</sup> cycles. NiO<sup>[40]</sup> materials can improve the ON/OFF ratio, while SiO<sub>2</sub><sup>[41]</sup> materials serve as a functional layer and greatly improve the data retention characteristics. Moreover, there are also a large number of binary oxides such as HfO<sub>2</sub><sup>[62]</sup> MnO<sub>2</sub>,<sup>[42]</sup> and so on.<sup>[63–65]</sup> Complex oxides generally have higher dielectric constants, such as Pr<sub>0.7</sub>Ca<sub>0.3</sub>MnO<sub>3</sub><sup>[66]</sup> (In 2000), SrTiO<sub>3</sub>,<sup>[44]</sup> BiFeO<sub>3</sub>,<sup>[45]</sup> LaAlO<sub>3</sub>,<sup>[49]</sup> and LiFePO<sub>4</sub>,<sup>[50]</sup> which can better improve switching parameters such as switching voltage and ON/OFF ratio. As early as 1976, Hirose et al.



**Figure 1.** Typical bipolar/unipolar *I*–*V* curves of RRAMs and their sandwich structure.

Resistance Switching Materials				
Organic Material		Inorganic Material		
Bioinspired	Polymers	Solid Electrolyte	Oxide	Low Dimension
				
Nanocellulose [22]	PVPCz59 [24]	GeS <sub>2</sub> [7]	SiO <sub>2</sub> [75]	Graphene [54]
				
Albumen [21]	PVDR [25]	Ag <sub>2</sub> Se [40]	SrTiO <sub>3</sub> [43]	Perovskite [61]
				
Proteins [82a]	PVK-C <sub>60</sub> [26]	Ge <sub>2</sub> Sb <sub>2</sub> Te <sub>5</sub> [57]	LaAlO <sub>3</sub> [49]	BN [58]
etc.	etc.	etc.	etc.	etc.

**Figure 2.** RRAM material classification example diagram. (Reproduced under a Creative Commons Attribution 4.0 International License.<sup>[21,22,82a]</sup> Copyright 2016, 2015, 2017, Springer Nature. Reproduced with permission.<sup>[24,25,40,54,75]</sup> Copyright 2012, 2010, 2012, 2015, 2012, Wiley-VCH. Reproduced with permission.<sup>[26,49,61]</sup> Copyright 2007, 2011, 2018, American Chemical Society. Reproduced with permission.<sup>[7]</sup> Copyright 2012, IEEE. Reproduced with permission.<sup>[43,57]</sup> Copyright 2004, 2012, Elsevier. Reproduced with permission.<sup>[58]</sup> Copyright 2017, Royal Society of Chemistry.)

studied an RRAM device using Ag-As<sub>2</sub>S<sub>3</sub> solid electrolyte material as a functional layer and observed single Ag conductive filaments by an optical microscope.<sup>[52]</sup> The researchers obtained good experimental results using complex electrolytes such as GeS<sub>2</sub>,<sup>[53]</sup> Ag<sub>2</sub>Se,<sup>[54]</sup> Ag-SbTe,<sup>[55]</sup> Cu-GeTe,<sup>[56]</sup> Ge<sub>2</sub>Sb<sub>2</sub>Te<sub>5</sub>,<sup>[57]</sup> etc.<sup>[67–73]</sup> At present, the emerging low-dimensional materials with small size and excellent physical properties have become a research hotspot in the field of small-sized electronic products.<sup>[58–61,74–81]</sup> A series of two-dimensional material (BN,<sup>[58,59]</sup> graphene,<sup>[74–77]</sup> MoS<sub>2</sub>,<sup>[78–81]</sup> and perovskites<sup>[60,61]</sup>) devices can achieve a switching ratio of about 10<sup>9</sup>, a current limit of 0.1 pico-Amperes, low power consumption, reduced operating voltage, enhanced ON/OFF resistance ratio, and endurance. The above description is a brief summary of the materials currently studied in the field of a resistive change memory, and the current material system needs further exploration and optimization.

### 3. Filament Mechanisms of RRAM Devices

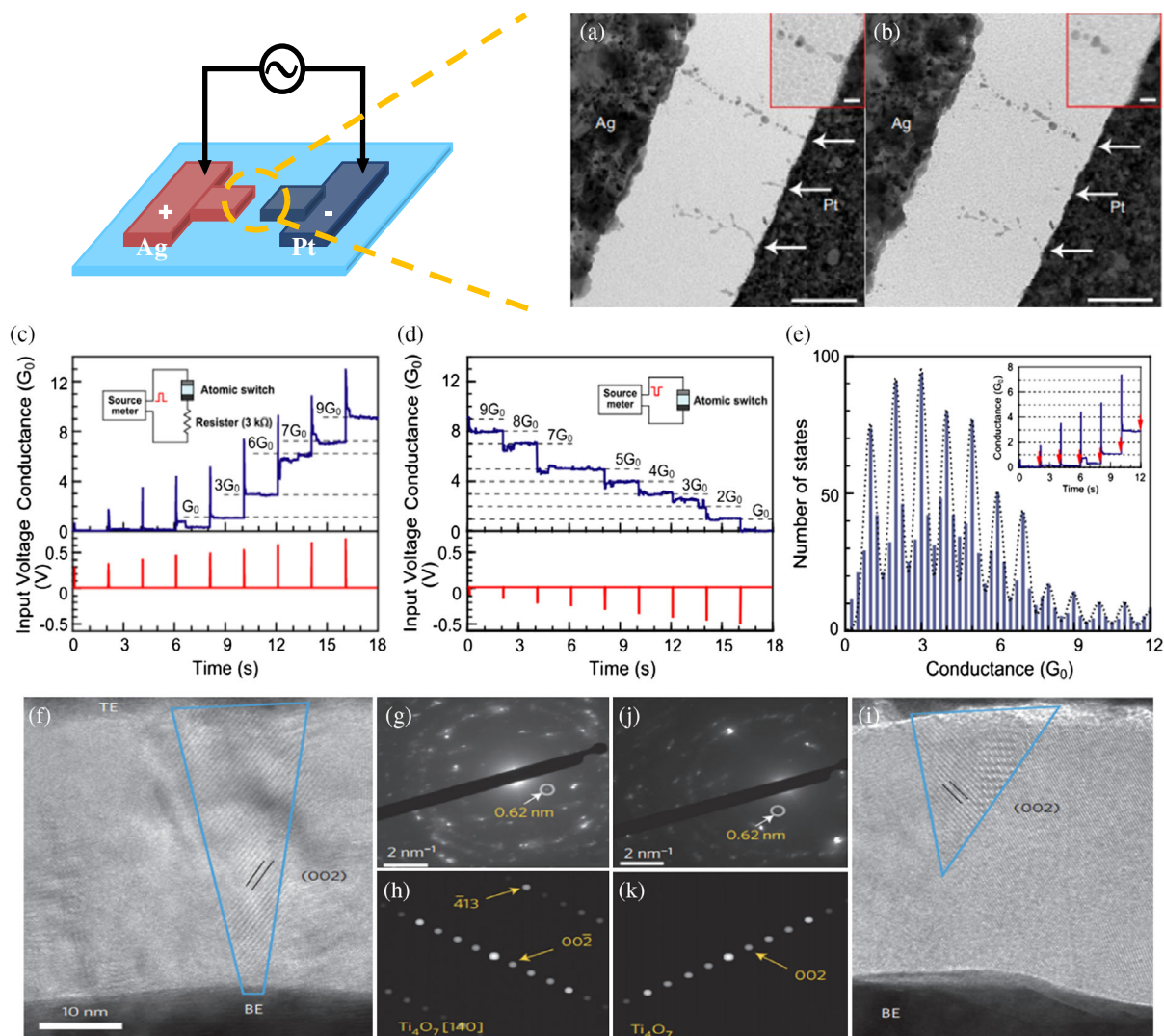
Although the resistive switching memory of different kinds of materials have been extensively studied to explain resistance change phenomena observed, the resistance switching mechanisms of RRAMs have been controversial. At present, the conductive filament mechanism is widely recognized, but there are still major disputes on key issues such as the microscopic process,

composition, and shape of the formation and destruction of the conductive filaments (CFs). One of the most commonly used classifications is based on the working principle of RRAM cells, which involves electrochemical metallization mechanism (ECM),<sup>[83]</sup> valence change mechanism (VCM),<sup>[84]</sup> and thermochemical mechanism (TCM).<sup>[85]</sup> The researchers demonstrated the conductive filament mechanism by analyzing the resistance change characteristics of the film material and the microstructure changes inside the films.

#### 3.1. Electrochemical Metallization Mechanism

The ECM is mostly used to explain the principle of devices with metal active electrodes with relatively high mobility, such as Ag, Cu, Ni, etc.<sup>[40,41,86–90]</sup> The formation of single Ag filaments of the Ag/Ag-As<sub>2</sub>S<sub>3</sub>/Au device was observed by an optical micrograph and reported in 1976 by Hirose.<sup>[52]</sup> Guo et al. used H<sub>2</sub>O as a solid electrolyte material and obtained SEM photographs of the growth process of Ag conductive filaments in lateral Ag/H<sub>2</sub>O/Pt devices, which visually proved the correctness of solid electrolyte theory.<sup>[91]</sup> Yang et al. observed the conductive filaments of the Pt/SiO<sub>2</sub>/Ag memory device by transmission electron microscopy (TEM), as shown in Figure 3a,b.<sup>[40]</sup> In the fresh planar device, conductive filaments are not formed in the SiO<sub>2</sub> layer between the Ag and Pt electrodes. When a positive voltage is applied to the Ag electrode,





**Figure 3.** a,b) Observation of conducting filament dynamics in SiO<sub>2</sub>-based RRAMs. c–e) Conductance quantization of the Ag/Ta<sub>2</sub>O<sub>5</sub>/Pt device: increase/decrease in quantized conductance under positive/negative voltage pulses (c,d). Histogram of the quantized conductance values extracted from the measured data (e). f–h) Magneli structures in the SET sample. High-resolution TEM image of a Ti<sub>4</sub>O<sub>7</sub> nanofilament (f), selected-area diffraction pattern of the film (g), and the corresponding simulated diffraction pattern (h). i–k) Disconnected Ti<sub>4</sub>O<sub>7</sub> structure in the conical shape; the images are presented in the same manner as those for the connected filaments. a,b) Reproduced with permission.<sup>[40]</sup> Copyright 2012, Springer Nature. c–e) Reproduced with permission.<sup>[91]</sup> Copyright 2012, IOP Publishing. f–k) Reproduced under a Creative Commons Attribution 4.0 International License.<sup>[63]</sup> Copyright 2016, Springer Nature.

the Ag electrode undergoes an oxidation reaction to produce Ag<sup>+</sup> (Ag → Ag<sup>+</sup> + e<sup>-</sup>). Ag<sup>+</sup> moves toward the Pt negative electrode under an electric field. When Ag<sup>+</sup> moves to the surface of the Pt electrode, it loses electrons and undergoes a reduction reaction to become Ag (Ag<sup>+</sup> + e<sup>-</sup> → Ag). As Ag builds up, Ag conductive filaments are formed in the resistive layer of RRAM; thus, the device exhibits a low resistance state as shown in Figure 3a. If a positive voltage is applied to the Pt electrode, the RRAM device is in a high resistance state (Figure 3b) owing to the broken conductive filament. Yan et al. investigated the resistance switching mechanism of Pt/SrTiO<sub>3</sub>/Ag memory devices by X-ray photoelectron spectroscopy (XPS) and indirectly proved Ag conductive filament mechanism in RRAM devices.<sup>[80]</sup> The device was placed in high and low resistance states, and the XPS depth profile of Ag and Pt elements was performed on the

device. The results show that the Ag elements always exist between the top Ag and Pt bottom electrode. Furthermore, a slight change in distribution intensity can be detected at different depths of the SrTiO<sub>3</sub> film when the device is in low resistance state. However, when the device is in the high resistance state, very little Ag element is detected in the SrTiO<sub>3</sub> medium film and the Pt film. Thus, the resistive switching behavior should be attributed to the formation and dissolution of the Ag filaments rather than to other physical mechanisms. Interestingly, Tsuruoka et al reported the Ag/Ta<sub>2</sub>O<sub>5</sub>/Pt cell with conductance quantization as shown in Figure 3c–e.<sup>[91]</sup> Long-term potentiation of biological synapses can be achieved by applying successive voltage pulses at periodic intervals of different time periods, indicating that oxide-based atomic switches have the potential to be used as neural computing systems.

### 3.2. Valence Change Mechanism

VCM and ECM mechanisms are similar, and both are related to electrochemical reactions and ion transport processes. ECM is normally an electrochemical reaction based on active metals, while VCM is an electrochemical reaction based on oxygen-related defects present in the oxide itself. In general, the device resistance change caused by the electrochemical reaction of oxygen-related defects was found in the oxide of functional layer materials. According to related reports, the transition between high resistance and low resistance states of RRAMs is caused by the rupture or formation of oxygen vacancy filament passages.<sup>[89,90,92–105]</sup> When a positive bias is applied to the inert top electrode, the oxide functional layer changes from a pristine state to a low resistance state, because the oxygen ions (O<sub>i</sub>) leave the original position, while the leftover oxygen vacancies gradually form a conductive path and drift toward the anode/functional layer interface. This process continues and eventually forms a conductive path consisting of oxygen vacancies (V<sub>o</sub>), which will increase the conductivity of the functional layer film. When the oxygen ions migrate back and the conductive channels inside the functional layer is destroyed by applying a reverse voltage, the RRAM device appears to have a high resistance state. Therefore, oxygen or oxygen vacancies might dominate the formation and destruction of conductive filaments in RRAM devices.

In 2007, Szot et al. reported the local conductivity of SrTiO<sub>3</sub> films using an atomic force microscope with a conducting tip; this indicated that SrTiO<sub>3</sub> films might achieve the bistable switching of the conductance between nonmetallic and metallic behaviors under an adequate electrical field.<sup>[99]</sup> Subsequently, the bipolar resistance switching behavior, which is caused by the perfect conductive nanochannels between the top layers of Pt under the influence of Ta-rich clusters, of the asymmetric TaO<sub>x</sub> was directly observed by the in situ detection method.<sup>[101]</sup> The VCM will generate the V<sub>o</sub>-O<sub>i</sub> anti-Frenkel pairs in general, but V<sub>o</sub>-O<sub>i</sub> anti-Frenkel pairs do not form the way it is presented in the paper.<sup>[2–4]</sup> In fact, even if they form, they will be unstable and will relax. Thus, the only way to form the device is to extract oxygen at the metal/oxide interface.

### 3.3. Thermochemical Mechanism

RRAM devices normally exhibit a tendency to resistance change when the electric field and Joule heat drive oxygen ion (or metal ion) reaction and migration predominates.<sup>[91,106]</sup> In the RRAM devices dominated by thermochemical reactions, the forming/set process corresponds to the thermal decomposition of the memory medium and consequent formation of the CFs, and the reset process is triggered by thermal melting of the existing conductive filaments.<sup>[107–111]</sup> Because Joule heating is independent of the electrode polarity, the unipolar/bipolar operation modes are effective in such RRAM cells. Therefore, non-polar switching of memory resistance is introduced in some literatures to describe this switching behavior. Jung et al reported the Pt/NiO/Pt device and clearly illustrated that by using the temperature dependence of the resistance switching transport in NiO films, the relative predominance in the off-state current can be determined by temperature and defect configuration. The

filaments in the Pt/TiO<sub>2</sub>/Pt system were directly detected during resistance change using a high-resolution transmission electron microscope (HTEM) as shown as in Figure 3c–f.<sup>[107]</sup> In situ current-voltage and low-temperature (130 K) conductivity measurements confirmed the formation and disruption of filaments of Ti<sub>n</sub>O<sub>2n–1</sub>. With the increase in oxygen vacancy concentration, a triangular region filament composed of Ti<sub>n</sub>O<sub>2n–1</sub> (Magneli phase) is gradually formed during the set process, as shown in Figure 3f. Figure 3g,h separately show the (002) spot of a Magneli phase, the fast fourier transform (FFT) image, and diffraction image-simulated diffraction pattern of Ti<sub>4</sub>O<sub>7</sub>, which coincides well with the FFT image. When acting through the thermal effect and the opposite external field, Ti<sub>n</sub>O<sub>2n–1</sub> returns to TiO<sub>2</sub> because a part of the triangular region filament recombines with the oxygen ions as shown in Figure 3i. The statement that “Joule heat often plays a leading role in the rupture of CFs of resistive switching memory” is widely accepted, but there is no direct experimental evidence to prove the factor responsible for the conductive filament formation process.

In fact, there are many factors that affect the formation and disruption of conductive filaments, including electrode size, electrode activity, and functional layer thickness.<sup>[112]</sup> On the other hand, different materials have different storage mechanisms for memory devices. The description presented above is only a summary of the filament mechanisms, and many other mechanisms have not been covered here in detail.<sup>[113–115]</sup> There is currently no consensus on the physical mechanism of the resistive switching phenomenon; therefore, it needs to be studied and explored in the future work.

## 4. Performance Optimization for RRAM

To manufacture reliable RRAMs that meet application requirements, excellent device performance is necessary. With the in-depth study of RRAMs, the performance parameters including the dispersed set/reset voltage distribution, low resistance ratio, high leakage current and data retention still need improvement. Studies on this topic have been conducted in recent years, and the statistical results show that the memory devices with different structures have large differences in performance, as shown in Table 1. The wide range of SET/RESET bias voltages offers the selective use of materials for both the conductive material and the electrode, depending on the application. The SET/RESET voltages are typically 0.2 to 3.05 V and –0.1 to –4 V, respectively, R<sub>OFF</sub>/R<sub>ON</sub> ratio is 10<sup>1</sup> to 10<sup>7</sup>, and cyclic endurance is in the range of 120 to >10<sup>12</sup>, depending on the materials chosen and the operating conditions. Currently, the memory characteristics are improved through three aspects: 1) “interface engineering” 2) element doping of functional materials, and 3) introduction of emerging low-dimensional materials.<sup>[82,118,119,121,127–134]</sup>

### 4.1. Interface Engineering

RRAM devices based on functional layers of metal oxides have attracted much attention due to their relatively stable performance. However, a thick oxide layer results in a higher programming voltage, and a thin oxide layer results in larger leakage current, dispersed SET/RESET voltage distribution, and small

**Table 1.** Statistics of performance parameters of different structural devices.

Device structure	$V_{\text{Forming}}$ [V]	$V_{\text{SET}}$ [V]	$V_{\text{RESET}}$ [V]	$R_{\text{OFF}}/R_{\text{ON}}$	Retention [s]	Endurance (cycle)	Reference
Pt/Ta <sub>2</sub> O <sub>5-x</sub> /Ta <sub>2</sub> O <sub>5-x</sub> /Pt	–	–1	2	–	–	>10 <sup>12</sup>	[116]
PEO/PAG/UCNPs	2	1.2–1.5	0.5–0.8	–	–	–	[103]
Metal/MgO/Co <sub>3</sub> O <sub>4</sub> /SiO <sub>2</sub> /Si	–	20	–10	10 <sup>3</sup>	10 <sup>4</sup>	10 <sup>8</sup>	[117]
Au/ZnO-CeO <sub>2</sub> /FTO	–	2.08	–1.9	10 <sup>2</sup>	>10 <sup>4</sup>	2×10 <sup>2</sup>	[118]
Au/Perovskite/G	7.6	2.8	≈–1	≈10	10 <sup>3</sup>	100	[119]
Au/CeO <sub>2</sub> /Au/Si	–	2.25	–2.56	10 <sup>2</sup>	2×10 <sup>4</sup>	10 <sup>4</sup>	[120]
Pt/TiO <sub>2</sub> :Ag/Pt	–	0.4–0.5	–0.3 to –0.2	–	–	–	[121]
Pt/a-COX/W/SiO <sub>2</sub> /Si	–	5	–4	10 <sup>4</sup>	10 <sup>4</sup>	4×10 <sup>4</sup>	[122]
Cu/CuO <sub>x</sub> /Cu/Au/Ti/SiO <sub>2</sub> /Si	1.7	1.3	–0.75	≈10 <sup>3</sup>	–	–	[63]
Glass/FTO/TiO <sub>x</sub> /Ag/TiO <sub>x</sub> /ITO	–	–0.5	0.2	2×10 <sup>2</sup>	10 <sup>4</sup>	10 <sup>2</sup>	[64]
Te/Ge <sub>2</sub> Sb <sub>2</sub> Te <sub>5</sub> /Pt/SiO <sub>2</sub> /Si	–	0.9–2.1	0.2–0.5	>10 <sup>2</sup>	–	20	[123]
TaN/CeO <sub>2</sub> /Ti/CeO <sub>2</sub> /Pt/SiO <sub>2</sub> /Si	1.8	–0.9 to –1.7	–1.5 to –0.8	10 <sup>3</sup>	10 <sup>4</sup>	>10 <sup>4</sup>	[124]
FEN/ITO/PSS/PI/Al	–	–0.5 to –0.7	2.5–3	4×10 <sup>3</sup>	10 <sup>4</sup>	10 <sup>2</sup>	[19]
Glass/ITO/AgG/Al	–	–1.2	2.1	105	–	–	[125]
Al/Si/Al/GQD/Al	2.2	–	–	116	10 <sup>4</sup>	–	[126]
ITO/MoS <sub>2</sub> /HfO <sub>x</sub> /ITO	–	–	–0.1	1.3×10 <sup>3</sup>	>10 <sup>4</sup>	2×10 <sup>2</sup>	[127]
TiN/HfO <sub>x</sub> /G	≈–4	0.2	–0.2	100	10 <sup>4</sup>	50	[102]
Au/NiO/Ni/NiO/Au	2	3.05	3.55	–	105	–	[128]
PET/ITO/GO-TiO <sub>2</sub> /Al	≈2.5	2.1	–0.5	10 <sup>2</sup>	–	–	[129]
FTO/TiO <sub>2</sub> /Ag	–3.4	–0.7	3.5	10	–	10 <sup>2</sup>	[82]
Ag/Nanocellulose/ITO	1.5	1	–0.5	10 <sup>7</sup>	>10 <sup>4</sup>	–	[22]
Glass/ITO/Proteins/Al	–1.2	–	–	10 <sup>3</sup>	10 <sup>4</sup>	5×10 <sup>2</sup>	[130]
Glass/Cr/Au/SA/Au	–	–1.3	1.4	>10 <sup>4</sup>	>10 <sup>4</sup>	–	[34]

window. Due to the physical limitations of the dimensions, an interface engineering was proposed to optimize the oxidized functional layer.<sup>[116,127,133,135]</sup> Interestingly, the metal/TiO<sub>2</sub>/metal conventional structure, in which a thin metal Ni layer is added to the top electrode interface and a barrier Al<sub>2</sub>O<sub>3</sub> layer is inserted into the bottom electrode interface, has a higher resistance ratio, bigger memory windows, and excellent endurance performance.<sup>[135]</sup> The Pt/TiO<sub>2</sub>/Al devices with inserted different active metals layers (Ni, Mn, and W) between the Pt top electrode and TiO<sub>2</sub> functional layers have a larger hysteresis and ON/OFF ratio than devices with the pure Pt top electrode. The phenomenon of an everlasting electrical breakdown did not appear in the devices with Al bottom electrode during a continuous scan cycles, so reveals that the bottom interface might also provide a stable performance. Lee et al. adjusted the symmetry of the conventional Pt/Ta<sub>x</sub>O<sub>y</sub>/Pt structure, reducing the leakage current of the device for a Schottky barrier formed between Pt and Ta<sub>2</sub>O<sub>5-x</sub>, and improving the characteristics of device endurance and switching speed.<sup>[116]</sup> They investigated the asymmetric *I*–*V* behavior of MIBM (Metal-Insulator-Base-Metal) and MBIM structures and the combined antisymmetric *I*–*V* behavior. Especially, for the combined structure of three kinds of devices, in voltage between –0.7 V and +0.7 V, the Schottky barrier depresses leakage current by being either reverse biased or biased below the forward threshold voltage. In addition to the above method of adding a buffer layer between the electrode and the

functional layer, an “interface engineering” method also needs to focus on the inside of the functional layer. Younis et al.<sup>[120]</sup> prepared an Au/CeO<sub>2</sub>/Au/Si device that achieves an ≈10<sup>4</sup> OFF/ON ratio and high uniformity, due to a large number of interfaces that result in an increase in the Vo concentration and improve the high probability of local Vo migration under the action of an electric field in the self-assembled CeO<sub>2</sub> nanocube.

## 4.2. Element Doping of Functional Materials

In addition to the interface engineering method, the doping of the oxide functional layer is an effective method for improving the uniformity, operation speed, and switching ratio of the device.<sup>[136–140]</sup> According to related reports, the performance of the functional layer of Al-doped ZnO is improved, mainly due to the formation of a dipole between the dopant and the oxygen vacancies, thereby reducing the formation energy and affecting the defect level<sup>[137]</sup>; doping Cu and Gd in the HfO<sub>2</sub> layer suppresses the random formation of oxygen vacancies, thereby largely improving device uniformity.<sup>[136,140]</sup> Adding one Pd-doped MoS<sub>2</sub> layer between the electrode and the functional layer of the traditional ITO/HfO<sub>2</sub>/ITO structure reduces the set voltage and improves uniformity, good stability, and memory window, which is magnified nearly 30 times.<sup>[133]</sup> Yan et al. performed silver doping using traditional titanium oxide materials to realize the RRAM performance improvement and memory-like artificial synaptic



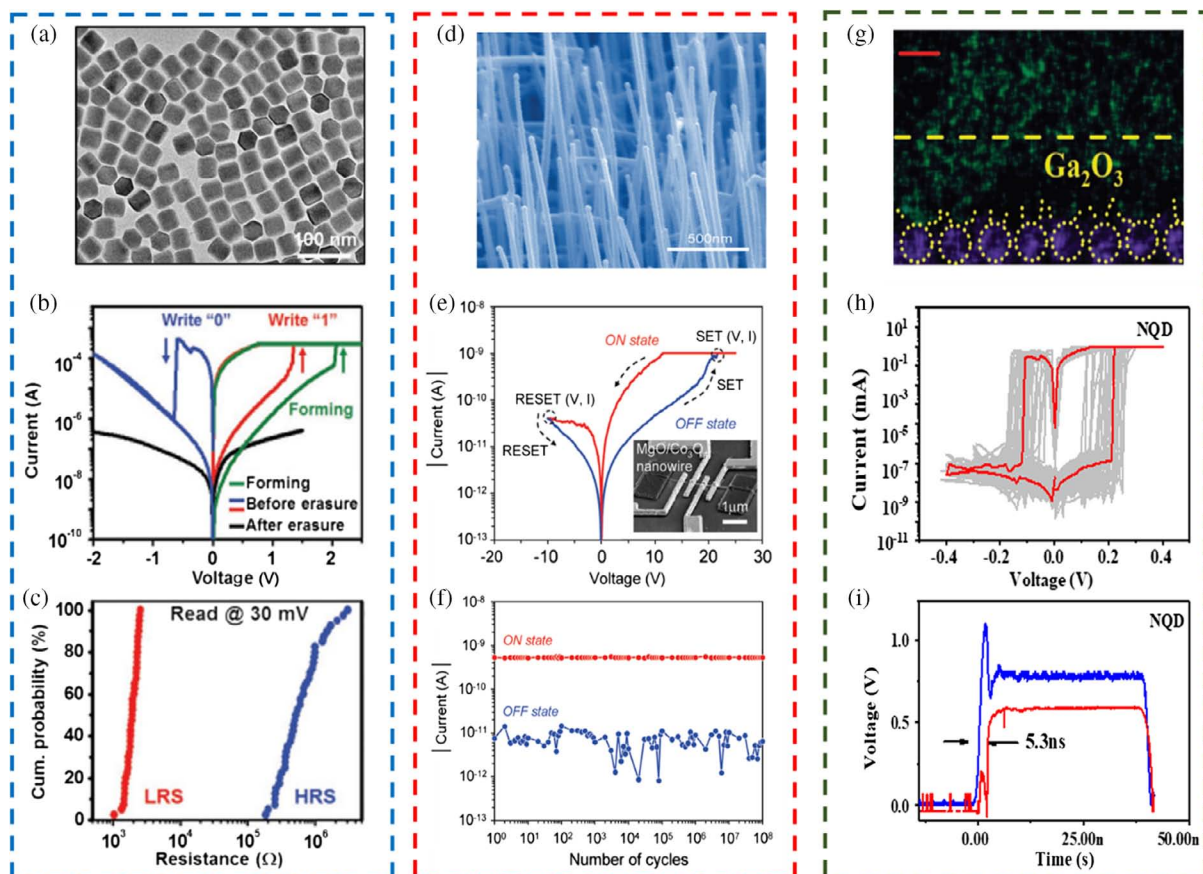
function.<sup>[121]</sup> Here, the enhanced memristor performance is achieved using a self-assembled Ag nanoclusters TiO<sub>2</sub> film formed by a gradient Ag dopant. The doping process is one of the main reasons why this method has received much attention.

#### 4.3. Introduction of Low-Dimensional Materials

When the traditional non-volatile memory is facing physical size limitations, the emerging low-dimensional materials are considered as potential materials for RRAM structures due to the small size of the dimension and their superior physical properties.<sup>[58,119,130,132–134,141,142]</sup> Lee et al. have reported that ultra-wideband multi-dye-sensitized upconverting nanoparticles (UCNPs, **Figure 4a**) were introduced to the flexible RRAM array with a UCNPs/photo-acid-generators (PAG)/poly(ethylene oxide) (PEO) layers for information security application.<sup>[103]</sup> Due to the ultra-thin nature of electronic devices, the entire system is deformable and can be integrated on a variety of curved surfaces, including human skin. **Figure 4b** exhibits the red/blue line curves that represent the unit device data writing “1” and erasing “0”, respectively, and the black curve represents the recoverable

data erasure after chemically dissolving the magnesium top electrode and the resistance transition layer. Nagashima et al. grew cobalt oxide (Co<sub>3</sub>O<sub>4</sub>) nanowires (**Figure 4d**) for RRAM device and achieved limiting current of 10<sup>−9</sup> A and endurance till 10<sup>8</sup> cycles.<sup>[117]</sup> Self-assembled nanowire RRAM offers an attractive solution for next-generation high-density nonvolatile memory, thereby reducing the device size beyond the limitation of current lithographic length scales. Nanowires can mimic the elongated shape of the nerve fiber morphology, have flexibility, and have a large area with good scalability; these characteristics enable the formation of a three-dimensional grid of nerve fibers in the human brain. More interestingly, Younis et al. applied a composite film of cerium oxide quantum dots (CeO<sub>2</sub> QDs) as surface charge traps and zinc oxide nanorods (ZnO NRs) to the resistive device.<sup>[118]</sup>

Yan et al. used a low-dimensional material of lead sulfide (PbS) as a functional material of RRAMs and systematically studied the electrical properties as shown in **Figure 4h,i**.<sup>[130]</sup> The self-assembled PbS, which can efficiently guide the growth direction for the CFs (**Figure 4g**), leads to enhanced performance such as reduced threshold voltage, uniformly distributed SET/RESET voltages, fast response time, and low power consumption.

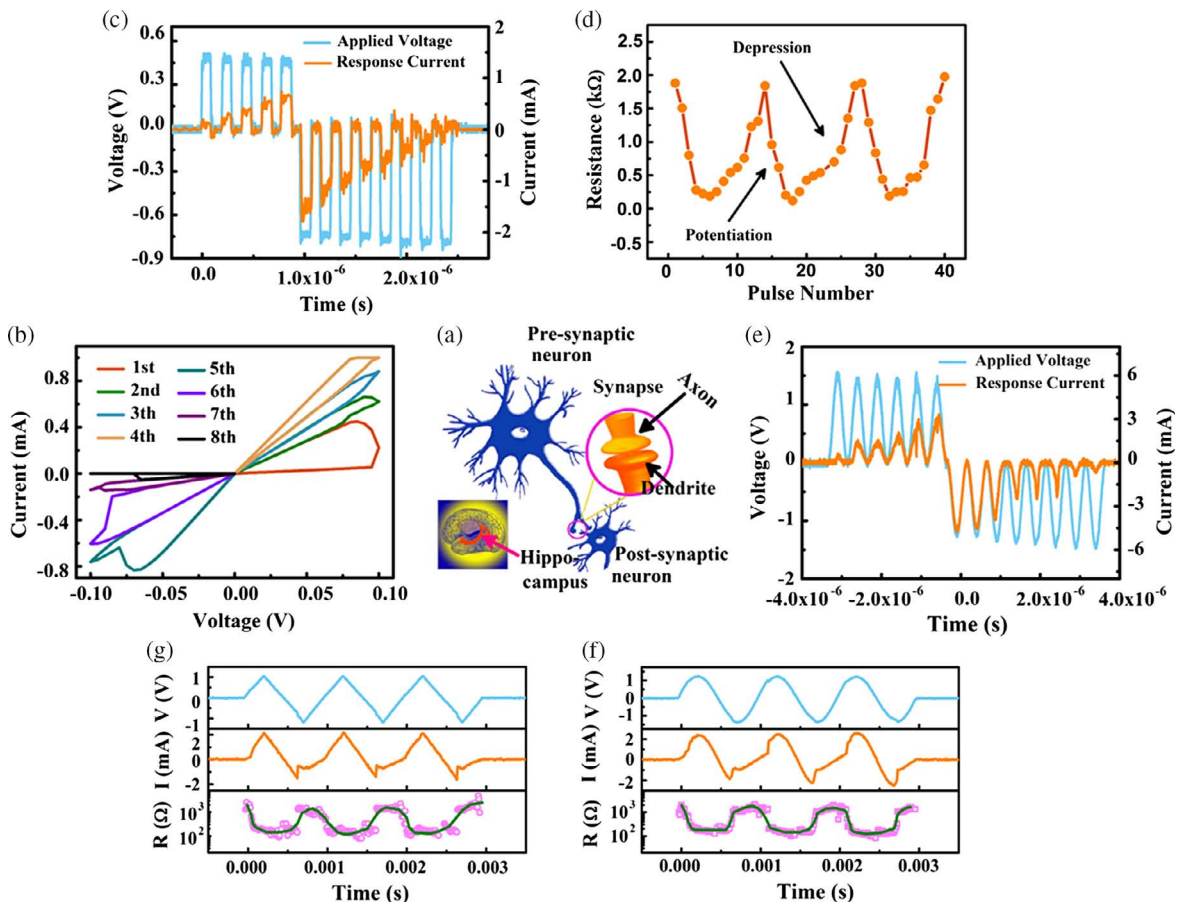


**Figure 4.** a) TEM image of the multi-dye-sensitized upconverting nanoparticles. b) *I*–*V* curve of the Cr/ZnO: Mn/Mg RRAM before and after photo-induced chemical destruction. c) Cumulative probability plot of resistances of low resistance state (LRS) and high resistance state (HRS) at read voltage of 30 mV. d) FESEM images of the MgO/Co<sub>3</sub>O<sub>4</sub> hetero-structured nanowires. e) Typical *I*–*V* characteristics of the individual MgO/Co<sub>3</sub>O<sub>4</sub> nanowire device. f) Switching endurance data of the MgO/Co<sub>3</sub>O<sub>4</sub> nanowire device. g) High-resolution TEM image of the device in “on” state. h) Endurance of *I*–*V* characteristics. i) SET response time. a–c) Reproduced with permission.<sup>[103]</sup> Copyright 2017, Wiley-VCH. d–f) Reproduced with permission.<sup>[117]</sup> Copyright 2010, American Chemical Society. g–i) Reproduced with permission.<sup>[130]</sup> Copyright 2018, Wiley-VCH.

**Table 2.** Comparison of the parameters of several kinds of memristors (table adapted from Yan et al.<sup>[76]</sup>).

Stack	Pulse scheme	Positive pulse voltage [V]	Negative pulse voltage [V]	Switching time
Pt/ $\alpha$ -IGZO/Pt	Identical pulse	5	−5	100 ns
Ag/MoO <sub>x</sub> /FTO	Identical pulse	4	−3	100 ns
W/HfO <sub>y</sub> /HfO <sub>x</sub> /Pt	Identical pulse	2.5	−2.5	50 ms
TiN/HfO <sub>x</sub> /AlO <sub>x</sub> /Pt	Incremental amplitude	2.2	−2.8	50 ns
Ag/PZT/LAMO	Identical pulse	2.2	−2.5	100 ns
Pd/WO <sub>x</sub> /W	Identical pulse	1.1	−1.1	1 ms
Pd/Ta <sub>2</sub> O <sub>5</sub> /TaO <sub>x</sub> /Pd	Identical pulse	1.1	−0.9	10 $\mu$ s
Co/BFO/CCMO	Identical pulse	1	−1.2	100 ns
TiN/TaO <sub>x</sub> /Pt	Identical pulse	0.82	−0.96	100 ns
Pt/TiO <sub>x</sub> /Pt	Identical pulse	0.8	−1.2	100 $\mu$ s
Pt/Ag/ZHO/GOQDs/ZHO/Ag	Identical pulse	0.6	−0.6	30 ns

Graphene oxide devices that can achieve the bidirectional progressive conductance were also used to reveal the impacts of different pulses on conductance control and the potential relationship between pulse modulation and energy applied; their performance parameters (switching time, pulse scheme, and voltage) are compared with others as shown in Table 2.<sup>[76]</sup> On the basis of the programming current statistics of RRAM functional materials in recent years, it is found that the programming current of the 2D-perovskite device can reach a minimum of 10 pico-Amperes, which is at least one order of magnitude lower than general RRAM devices, thus achieving the goal of low power consumption.<sup>[129]</sup> Due to the extremely low programming current, the resistive switching memory demonstrated 400 fJ/spike synaptic operation, which is very close to the energy consumption of biological synapses. The 2D-BN devices show the coexistence of forming free bipolar and threshold-type resistive switching (RS) with low sweeping voltages of 0.4 V, owing to the penetration of metallic ions from adjacent electrodes in the grain boundaries in the polycrystalline BN stack.<sup>[58]</sup> At present, it is reported that the size of the low-dimensional material is relatively large, and the size of the actually integrated RRAM cell device is very small; thus, the low-dimensional material of a



**Figure 5.** Memristive behaviors. a) Schematic illustration of synaptic plasticity modulation. b) The obviously down-up and up-down evolution of conduction as biological synapse. c) The modulation of conduction by pulse train mode. d) Repeated properties of conductance modulation. e) The applied voltage is  $\pm v_0 \sin^2(\omega_0 t)$ . f) AC model stimulation. g) DC model stimulation. a–g) Reproduced with permission.<sup>[133]</sup> Copyright 2018, Wiley-VCH.



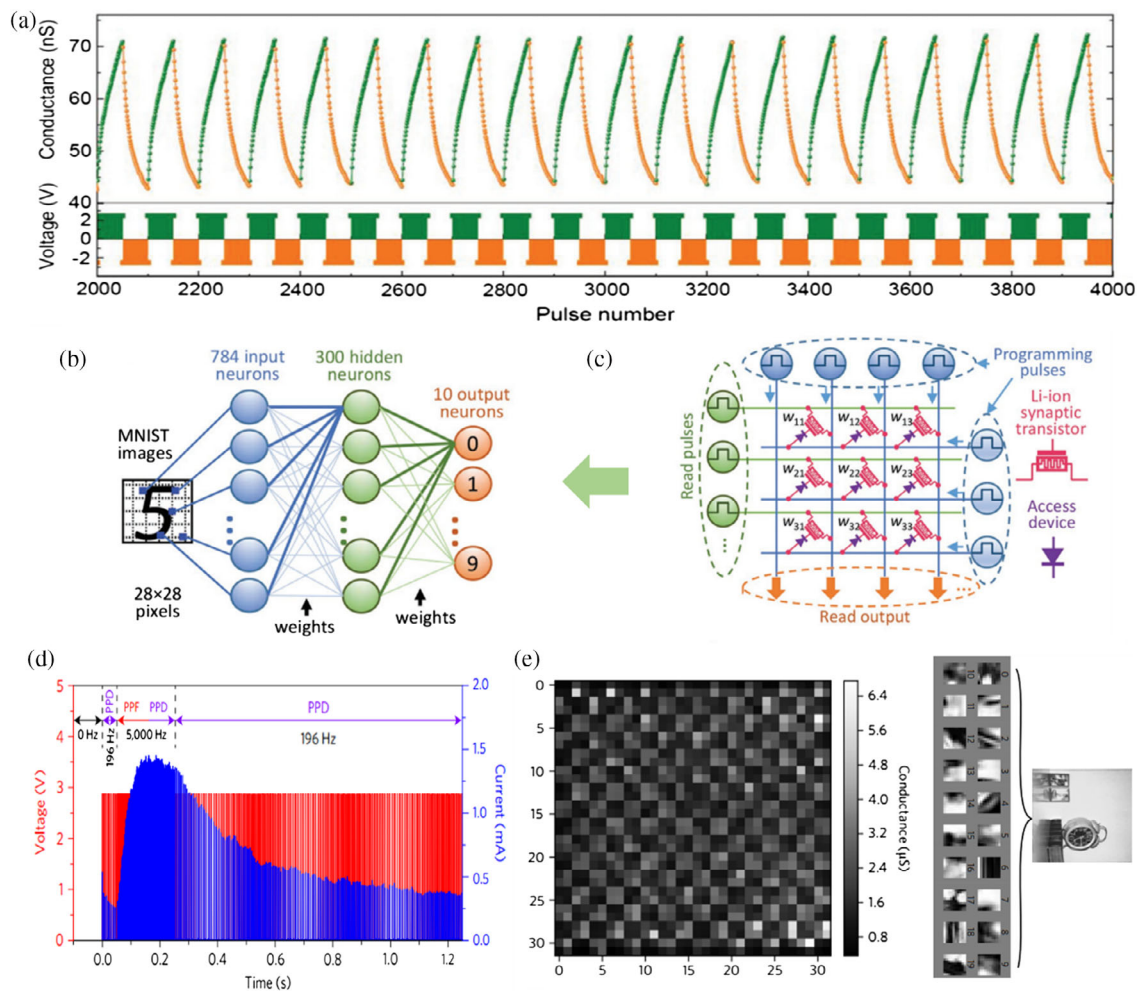
smaller size is the current development direction for the improvement of high-density storage area of RRAMs. Furthermore, the performance reliability of the low-dimensional RRAM and large-area growth process technology for low-dimensional materials remain difficult problems that need to be solved in the future.

## 5. Application Prospects

Due to its superior electrical characteristics such as high speed, low power consumption, and high density, RRAM with a simple structure has good application prospects in neuromorphic computing systems and conventional memory computing systems mainly involved in field programmable gate array,<sup>[144]</sup> nanotechnology, and traditional CMOS process hybrid integration<sup>[145]</sup>. It is worth noting that the neuromorphic computing systems-based multiple value RRAM devices are expected to overcome the shortcomings of the von Neumann architecture computing

platforms and provide high efficiency for data centric applications in the big data era.<sup>[3,58,128,133,146–150]</sup>

Calcium ions ( $\text{Ca}^{2+}$ ) play a crucial role in the transmission of information between the presynaptic and postsynaptic membrane of biological synapses. Researchers have found that the accumulation and diffusion of silver ions ( $\text{Ag}^+$ ) in the RRAM functional layer might simulate this passing process of biological information under the pulse sweeping voltages. **Figure 5a** depicts a schematic representation of synapses responsible for memory and learning in the human brain, consisting of axons and dendrites.<sup>[133]</sup> The formation and cleavage of the silver conductive filaments of the  $\text{Ag}/\text{TiO}_2$ :  $\text{Ag}/\text{Pt}$  structures can better simulate the bio-synaptic calcium ion information transmission. The memory device gradually shows enhancement and inhibition of conduction under positive and negative pulse sequences, which can completely simulate the excitation and inhibition of biological synapse. Figure 5b clearly shows that the memory conductance gradually increases (or decreases) under positive



**Figure 6.** RRAM applications. a) Analog channel conductance modulation under 50 repeated positive and gate voltage pulses. Schematics of a b) three-layer neural network and c) a synaptic weight layer composed of voltage programmed Li-ion synaptic transistor crossbar array and access devices. d) Short-term synaptic plasticity exhibited by a single diffusive memristor. e) A  $32 \times 32$  chequerboard pattern (schematic of the sparse coding concept). a–c) Reproduced with permission.<sup>[150]</sup> Copyright 2018, Wiley-VCH. d) Reproduced with permission.<sup>[3]</sup> Copyright 2016, Springer Nature. e) Reproduced with permission.<sup>[3]</sup> Copyright 2017, Springer Nature.

(or negative) scan voltages. Thus, the memory resistance can be regulated by a direct current voltage. More interestingly, the conductance can be continuously controlled by the subsequently applied sinusoidal voltage, instead of the pulse as shown in Figure 5e. RRAMs with the characteristics of both short-term and long-term plasticity for ion diffusion, such as paired-pulse facilitation (PPF) (conductance increase), paired-pulse depression (PPD) (conductance decrease), and spiking-time-dependent plasticity (STDP), can mimic the neuromorphic information transmission of several brain functionalities process, mainly involving voice and image recognition by utilizing the deep learning algorithm, and might be applied to crossbar array-based computing hardware system as shown in Figure 6.<sup>[3,149,150]</sup>

However, on the road to commercial use and mass production, the process of resistive switching memory still has many problems related to the uniformity of resistance change memory parameters and failure mechanisms.<sup>[143,151–154]</sup> For example, the high/low resistance states, the SET/RESET currents, and the operating voltages of RRAMs usually illustrate the discrepancy from cell to cell and from cycle to cycle. In addition, when the resistive switching memory is integrated in three-dimensional high-density circuits, the elimination of leakage current paths in the cross array is urgently needed. Further development of low-cost, easy-to-manufacture RRAM technologies will likely pave the way for the future.<sup>[155,156]</sup>

## Acknowledgements

This work was financially supported by the National Natural Science Foundation of China (Grant Nos. 61674050 and 61874158), the Top-notch Youth Project in Hebei Province (Grant No. BJ2014008), the Outstanding Youth Project of Hebei Province (Grant No. F2016201220), the Outstanding Youth Cultivation Project of Hebei University (Grant No. 2015JQY01), the Project of Science and Technology Activities for Overseas Researcher (Grant No. CL201602), the Institute of Baoding Nanyang Research-New Material Technology Platform (Grant No. 17H03), the Project of Distinguished Young of Hebei Province (Grant No. A2018201231), the Training Program of Innovation and Entrepreneurship for Undergraduates (Grant Nos. 201710075013 and 2017075), the Support Program for the Top Young Talents of Hebei Province (Grant No. 70280011807), Training and Introduction of High-level Innovative Talents of Hebei University (Grant No. 801260201300), Innovation Funding Project of Hebei Province (Grant No. CXZZBS2019030), Innovation Funding Project of Hebei University (Grant No. hbu2019ss004), and Hundred Persons Plan of Hebei Province (No. 606999919001).

## Conflict of Interest

The authors declare no conflict of interest.

## Keywords

filament mechanism, materials design, performance optimization, resistive random access memory

Received: February 5, 2019

Revised: April 29, 2019

Published online:

[1] C. Wolf, D. E. J. Linden, *Genes, Brain Behav.* **2012**, *11*, 3.

[2] D. Ielmini, H. S. P. Wong, *Nat. Electr.* **2018**, *1*, 333.

- [3] Z. Wang, S. Joshi, S. E. Savel'Ev, H. Jiang, R. Midya, P. Lin, M. Hu, N. Ge, J. P. Strachan, Z. Li, Q. Wu, M. Barnell, G.-L. Li, H. L. Xin, R. S. Williams, Q. Xia, J. J. Yang, *Nat. Mater.* **2017**, *16*, 101.
- [4] M. A. Lastras-Montano, K. T. Cheng, *Nat. Electr.* **2018**, *1*, 466.
- [5] Z. Jun, *Int. Conf. Solid-State Integr. Circuit Technol.* **2001**, *1*, 189.
- [6] H. Wang, D. Ren, C. Lu, X. Yan, *Appl. Phys. Lett.* **2018**, *112*, 231903.
- [7] E. Vianello, C. Cagli, G. Molas, E. Souchier, P. Blaise, C. Carabasse, G. Rodriguez, V. Jousseume, B. De Salvo, F. Dahmani, P. Verrier, D. Bretegnier, J. Liebault, in *2012 Proc. of the ESSDERC, IEEE, Piscataway, NJ* **2012**, pp. 278–281.
- [8] D. S. Jeong, K. M. Kim, S. Kim, B. J. Choi, C. S. Hwang, *Adv. Electr. Mater.* **2016**, *2*, 1600090.
- [9] Y. Song, D. Yoo, T. Lee, *J. Korean. Phys. Soc.* **2018**, *73*, 479.
- [10] R. Bez, A. Pirovano, *Mater. Sci. Semicond. Process.* **2004**, *7*, 349.
- [11] R. Bez, E. Camerlenghi, A. Modelli, A. Visconti *Proc. IEEE* **2003**, *91*, 489.
- [12] J. G. Simmons, R. R. Verderber *Proc. R. Soc. Lond. A* **1967**, *301*, 77.
- [13] S. Chen, Z. Lou, D. Chen, G. Shen, *Adv. Mater.* **2018**, *30*, 1705400.
- [14] X. Yan, Z. Zhou, B. Ding, J. Zhao, Y. Zhang, *J. Mater. Chem. C* **2017**, *5*, 2259.
- [15] X. Yan, H. Hao, Y. Chen, S. Shi, E. Zhang, J. Lou, B. Liu, *Nanoscale Res. Lett.* **2014**, *9*, 548.
- [16] Y. Li, Y. Zhong, L. Xu, J. Zhang, X. Xu, H. Sun, X. Miao, *Sci. Rep.* **2013**, *3*, 1619.
- [17] K. I. Chou, C. H. Cheng, Z. W. Zheng, M. Liu, A. Chin, *IEEE Electron. Device Lett.* **2013**, *34*, 505.
- [18] A. Younis, S. Li, *RSC Adv.* **2018**, *8*, 28763.
- [19] M. K. Choi, W. K. Kim, S. Sung, C. Wu, T. W. Kim, *Sci. Rep.* **2018**, *8*, 12275.
- [20] Y. Xing, C. Shi, J. Zhao, W. Qiu, N. Lin, J. Wang, X. B. Yan, W. D. Yu, X. Y. Liu, *Small* **2017**, *13*, 1702390.
- [21] Y. C. Chen, H. C. Yu, C. Y. Huang, W. L. Chung, S. L. Wu, Y. K. Su, *Sci. Rep.* **2015**, *5*, 10022.
- [22] U. Celano, K. Nagashima, H. Koga, M. Nogi, F. Zhuge, G. Meng, Y. He, J. D. Boeck, M. Jurczak, W. Vandervorst, T. Yanagida, *NPG Asia Mater.* **2016**, *8*, e310.
- [23] B. Ibarlucea, T. F. Akbar, K. Kim, T. Rim, C. K. Baek, A. Ascoli, R. Tetzlaff, L. Baraban, G. Cuniberti, *Nano. Res.* **2018**, *11*, 1057.
- [24] N. G. Kang, B. Cho, B. G. Kang, S. Song, T. Lee, J. S. Lee, *Adv. Mater.* **2012**, *24*, 385.
- [25] X. D. Zhuang, Y. Chen, G. Liu, B. Zhang, K. G. Neoh, E. T. Kang, C. X. Zhu, Y. X. Li, L. J. Niu, *Adv. Funct. Mater.* **2010**, *20*, 2916.
- [26] Q. D. Ling, S. L. Lim, Y. Song, C. X. Zhu, D. S. H. Chan, E. T. Kang, K. G. Neoh, *Langmuir* **2007**, *23*, 312.
- [27] D. I. Son, T. W. Kim, J. H. Shim, J. H. Jung, D. U. Lee, J. M. Lee, W. K. Choi, *Nano. Lett.* **2010**, *10*, 2441.
- [28] L. V. Gregor, *IBM J. Res. Dev.* **1968**, *12*, 140.
- [29] L. V. Gregor, *Thin Solid Films* **1968**, *2*, 235.
- [30] S. Gao, C. Song, C. Chen, F. Zeng, F. Pan, *J. Mater. Chem. C* **2012**, *116*, 17955.
- [31] C. W. Chu, J. Ouyang, J. H. Tseng, Y. Yang, *Adv. Mater.* **2015**, *17*, 1440.
- [32] M. V. Jacob, D. Taguchi, M. Iwamoto, K. Bazaka, R. S. Rawat, *Carbon* **2017**, *112*, 111.
- [33] X. Liu, Z. Ji, D. Tu, L. Shang, J. Liu, M. Liu, C. Xie, *Org. Electron.* **2009**, *10*, 1191.
- [34] D. K. Maiti, S. Debnath, S. M. Nawaz, B. Dey, E. Dinda, D. Roy, S. Ray, A. Mallik, S. A. Hussain, *Sci. Rep.* **2017**, *7*, 13308.
- [35] L. D. Bozano, B. W. Kean, M. Beinhoff, K. R. Carter, P. M. Rice, J. C. Scott, *Adv. Funct. Mater.* **2015**, *15*, 1933.
- [36] W. Bai, R. Huang, Y. Cai, Y. Tang, X. Zhang, Y. Wang, *IEEE Electron Device Lett.* **2013**, *34*, 223.
- [37] K. H. Kim, S. Gaba, D. Wheeler, J. M. Cruz-Albrecht, T. Hussain, N. Srinivasa, W. Lu, *Nano Lett.* **2011**, *12*, 389.

- [38] T. W. Hickmott, *J. Appl. Phys.* **1962**, 33, 2669.
- [39] D. P. Sahu, S. N. Jammalamadaka, *Sci. Rep.* **2017**, 7, 17224.
- [40] Y. Yang, P. Gao, S. Gaba, T. Chang, X. Pan, W. Lu, *Nat. Commun.* **2012**, 3, 732.
- [41] Y. H. Ting, J. Y. Chen, C. W. Huang, T. K. Huang, C. Y. Hsieh, W. W. Wu, *Small* **2018**, 14, 1703153.
- [42] M. K. Yang, J. W. Park, T. K. Ko, J. K. Lee, *Appl. Phys. Lett.* **2009**, 95, 5655.
- [43] E. Celik, Y. Yamada, I. Hirabayashi, Y. Shiohara, *Mater. Sci. Eng. B* **2004**, 110, 94.
- [44] X. B. Yan, Y. D. Xia, H. N. Xu, X. Gao, H. T. Li, J. Yin, Z. G. Liu, *Appl. Phys. Lett.* **2010**, 97, 112101.
- [45] J. H. Jeon, H. Y. Joo, Y. M. Kim, D. H. Lee, J. S. Kim, Y. A. Kim, T. Choi, B. H. Park, *Sci. Rep.* **2016**, 6, 23299.
- [46] C. Kumari, I. Varun, S. P. Tiwari, A. Dixit, *Superlattices Microstruct.* **2018**, 120, 67.
- [47] S. Yao, S. Zhou, C. Wu, W. Zhang, D. Bürger, S. Slesazek, T. Mikolajick, M. Helm, H. Schmidt, *Appl. Phys. Express* **2012**, 4, 095802.
- [48] Z. Zhou, X. Yan, J. Zhao, C. Lu, D. Ren, N. Lu, J. Wang, L. Zhang, X. Li, H. Wang, M. Zhao, *J. Mater. Chem. C* **2019**, 7, 1561.
- [49] X. Yang, H. Su, *ACS Appl. Mater. Interfaces* **2011**, 3, 3819.
- [50] L. Zhang, C. Wu, J. Liu, X. Zhao, Z. Wang, H. Xu, Y. Liu, *Phys. Status Solidi RRL* **2018**, 12, 1800320.
- [51] X. Yan, Z. Zhou, J. Zhao, Q. Liu, H. Wang, G. Yuan, J. Chen, *Nano. Res.* **2018**, 11, 1183.
- [52] Y. Hirose, H. Hirose, *J. Appl. Phys.* **1976**, 47, 2767.
- [53] F. Longnos, E. Vianello, C. Cagli, G. Molas, E. Souchier, P. Blaise, C. Carabasseb, G. Rodriguezb, V. Jousseameb, B. DeSalvob, F. Dahmania, P. Verriera, D. Bretegniera, J. Liebault, *Solid-State Electron.* **2013**, 84, 155.
- [54] J. Jang, F. Pan, K. Braam, V. Subramanian, *Adv. Mater.* **2012**, 24, 3573.
- [55] Y. S. Park, S. Y. Lee, M. Jang, S. M. Yoon, *Electron. Lett.* **2012**, 48, 458.
- [56] S. J. Choi, G. S. Park, K. H. Kim, S. Cho, W. Y. Yang, X. S. Li, J. H. Moon, K. J. Lee, K. Kim, *Adv. Mater.* **2011**, 23, 3272.
- [57] D. Deleruyelle, M. Putero, T. Ouled-Khachroum, M. Bocquet, M. V. Coulet, X. Boddaert, C. Calmes, C. Mullera, *Solid-State Electron.* **2013**, 79, 159.
- [58] G. U. Siddiqui, M. M. Rehman, Y. J. Yang, K. H. Choi, *J. Mater. Chem. C* **2017**, 5, 862.
- [59] K. Qian, R. Y. Tay, V. C. Nguyen, J. Wang, G. Cai, T. Chen, E. H. T. Teo, P. S. Lee, *Adv. Fun. Mater.* **2016**, 26, 2176.
- [60] H. Tian, L. Zhao, X. Wang, Y. W. Yeh, N. Yao, B. P. Rand, T. L. Ren, *ACS Nano* **2017**, 11, 12247.
- [61] M. Kumar, H. S. Kim, D. Y. Park, M. S. Jeong, J. Kim, *ACS Appl. Mater. Interfaces* **2018**, 10, 12768.
- [62] J. Liu, H. Yang, Z. Ma, K. Chen, X. Zhang, X. Huang, S. Oda, *J. Phys. D: Appl. Phys.* **2017**, 51, 025102.
- [63] U. B. Han, J. S. Lee, *Sci. Rep.* **2016**, 6, 25537.
- [64] Y. J. Huang, S. C. Chao, D. H. Lien, C. Y. Wen, J. H. He, S. C. Lee, *Sci. Rep.* **2016**, 6, 23945.
- [65] X. Guo, C. Schindler, S. Menzel, R. Waser, *Appl. Phys. Lett.* **2007**, 91, 133513.
- [66] S. D. Q. Liu, N. J. Wu, A. Ignatiev, *Appl. Phys. Lett.* **2000**, 76, 2749.
- [67] M. N. Kozicki, M. Park, M. Mitkova *IEEE Trans. Nanotechnol.* **2005**, 4, 331.
- [68] T. Sakamoto, H. Sunamura, H. Kawaura, T. Hasegawa, T. Nakayama, M. Aono, *Appl. Phys. Lett.* **2003**, 82, 3032.
- [69] K. Terabe, T. Hasegawa, T. Nakayama, M. Aono, *Nature* **2005**, 433, 47.
- [70] S. Kaeriyama, T. Sakamoto, H. Sunamura, M. Mizuno, H. Kawaura, T. Hasegawa, K. Terabe, T. Nakayama, M. Aono, *IEEE J. Solid-State Circuits* **2005**, 40, 168.
- [71] N. Banno, T. Sakamoto, T. Hasegawa, K. Terabe, M. Aono, *Jpn. J. Appl. Phys.* **2006**, 45, 3666.
- [72] M. N. Kozicki, M. Balakrishnan, C. Gopalan, C. Ratnakumar, M. Mitkova, in *Proc. IEEE Non-Volatile Memory Technology Symp.* Dallas, TX, Nov **2005**, p. 83.
- [73] Z. Wang, P. B. Griffin, J. McVittie, S. Wong, P. C. McIntyre, Y. Nishi, *IEEE Electron Device Lett.* **2007**, 28, 14.
- [74] X. F. Cheng, X. Hou, J. Zhou, B. J. Gao, J. H. He, H. Li, J. M. Lu, *Small* **2018**, 14, 1703667.
- [75] M. H. Jang, H. D. Ha, E. S. Lee, F. Liu, Y. H. Kim, T. S. Seo, Y. H. Cho, *Small* **2015**, 11, 3772.
- [76] X. Yan, L. Zhang, H. Chen, X. Li, J. Wang, Q. Liu, C. Lu, J. Chen, H. Wu, P. Zhou, *Adv. Fun. Mater.* **2018**, 28, 1803728.
- [77] C. Hao, F. Wen, J. Xiang, S. Yuan, B. Yang, L. Li, W. Wang, Z. Zeng, L. Wang, Z. Liu, Y. Tian, *Adv. Funct. Mater.* **2016**, 26, 2016.
- [78] R. Chen, C. Lin, H. Yu, Y. Tang, C. Song, L. Yuwen, H. Li, X. Xie, L. Wang, W. Huang, *Chem. Mater.* **2016**, 28, 4300.
- [79] L. Yang, K. Majumdar, H. Liu, Y. Du, H. Wu, M. Hatzistergos, P. Y. Hung, R. Tieckelmann, W. Tsai, C. Hobbs, P. D. Ye, *Nano. Lett.* **2014**, 14, 6275.
- [80] C. Yeon, S. J. Yun, J. Yang, D. H. Youn, J. W. Lim, *Small* **2018**, 14, 1702747.
- [81] P. Zhang, C. Gao, B. Xu, L. Qi, C. Jiang, M. Gao, D. Xue, *Small* **2016**, 12, 2077.
- [82] a) L. Wang, D. Wen, *Sci. Rep.* **2017**, 7, 17418; b) D. P. Sahu, S. N. Jammalamadaka, *Sci. Rep.* **2017**, 7, 17224.
- [83] M. N. Kozicki, M. Mitkova, *Nanotechnology*, Vol. 3 (Ed: R. Waser), Wiley-VCH, Weinheim **2008**.
- [84] R. Oligschlaeger, R. Waser, R. Meyer, S. Karthaus, R. Dittmann, *Appl. Phys. Lett.* **2006**, 88, 42901.
- [85] L. Nagarajan, R. A. De Souza, D. Samuelis, I. Valov, A. Borger, J. Janek, K. D. Becker, P. C. Schmidt, M. Martin, *Nat. Mater.* **2008**, 7, 391.
- [86] X. F. Cheng, X. Hou, J. Zhou, B. J. Gao, J. H. He, H. Li, Q. F. Xu, N. J. Li, D. Y. Chen, J. M. Lu, *Small* **2018**, 14, 1703667.
- [87] S. U. Sharath, S. Vogel, L. Molina-Luna, E. Hildebrandt, C. Wenger, J. Kurian, M. Duerrschabel, T. Niermann, G. Niu, P. Calka, M. Lehmann, H. J. Kleebe, T. Schroeder, L. Alff, *Adv. Fun. Mater.* **2017**, 27, 1700432.
- [88] X. B. Yan, K. Li, J. Yin, Y. D. Xia, H. X. Guo, L. Chen, Z. G. Liu, *Electrochem. Solid-State Lett.* **2010**, 13, H87.
- [89] G. S. Park, X. S. Li, D. C. Kim, R. J. Jung, M. J. Lee, S. Seo, *Appl. Phys. Lett.* **2007**, 91, 222103.
- [90] D. H. Kwon, K. M. Kim, J. H. Jang, J. M. Jeon, M. H. Lee, G. H. Kim, X. S. Li, G. S. Park, B. Lee, S. Han, M. Kim, C. S. Hwang, *Nat. Nanotechnol.* **2010**, 5, 148.
- [91] T. Tsuruoka, T. Hasegawa, K. Terabe, M. Aono, *Nanotechnology* **2012**, 23, 435705.
- [92] W. Xue, G. Liu, Z. Zhong, Y. Dai, J. Shang, Y. Liu, H. Yang, X. Yi, H. Tan, L. Pan, S. Gao, J. Ding, X. H. Xu, R. W. Li, *Adv. Mater.* **2017**, 29, 1702162.
- [93] X. Guo, C. Schindler, *Appl. Phys. Lett.* **2007**, 91, 133513.
- [94] Z. Wei, Y. Kanzawa, K. Arita, Y. Katoh, K. Kawai, S. Muraoka, S. Mitani, S. Fujii, K. Katayama, M. Iijima, T. Mikawa, T. Ninomiya, R. Miyana, Y. Kawashima, K. Tsuji, A. Himeno, T. Okada, R. Azuma, K. Shimakawa, H. Sugaya, T. Takagi, R. Yasuhara, K. Horiba, H. Kumigashira, M. Oshima, *IEEE Int. Electron Dev. Meet. Tech. Dig.* **2008**, 293, 5671467.
- [95] A. E. McHale, H. L. Tuller, *J. Am. Ceram. Soc.* **1985**, 68, 646.
- [96] C. C. Lin, B. C. Tu, C. C. Lin, C. H. Lin, T. Y. Tseng, *IEEE Electr. Device Lett.* **2006**, 27, 725.
- [97] R. Muenstermann, T. Menke, R. Dittmann, R. Waser, *Adv. Mater.* **2010**, 22, 4819.



- [98] K. Szot, R. Dittmann, W. Speier, R. Waser, *Phys. Status Sol. (RRL)-Rapid Res. Lett.* **2007**, 1, R86.
- [99] K. Szot, W. Speier, G. Bihlmayer, R. Waser, *Nat. Mater.* **2006**, 5, 312.
- [100] R. Waser, M. Aono, *Nat. Mater.* **2007**, 6, 833.
- [101] G. S. Park, Y. B. Kim, S. Y. Park, X. S. Li, S. Heo, M. J. Lee, *Nat. Commun.* **2013**, 4, 2382.
- [102] S. Lee, J. Sohn, Z. Jiang, H. Y. Chen, H. S. P. Wong, *Nat. Commun.* **2015**, 6, 8407.
- [103] J. Lee, B. Yoo, H. Lee, G. D. Cha, H. S. Lee, Y. Cho, S. Y. Kim, H. Seo, W. Lee, D. Son, M. Kang, H. M. Kim, Y. Park, T. Hyeon, D. H. Kim, *Adv. Mater.* **2017**, 29, 1603169.
- [104] S. Munjal, N. Khare, *Sci. Rep.* **2017**, 7, 12427.
- [105] S. K. Pradhan, B. Xiao, S. Mishra, A. Killam, A. K. Pradhan, *Sci. Rep.* **2016**, 6, 26763.
- [106] S. Gao, F. Zeng, C. Chen, G. Tang, Y. Lin, Z. Zheng, C. Song, F. Pan, *Nanotechnology* **2013**, 24, 335201.
- [107] D. H. Kwon, K. M. Kim, J. H. Jang, J. M. Jeon, M. H. Lee, G. H. Kim, X. S. Li, G. S. Park, B. Lee, S. Han, M. Kim, C. S. Hwang, *Nat. Nanotechnol.* **2010**, 5, 148.
- [108] R. Waser, R. Dittmann, G. Staikov, K. Szot, *Adv. Mater.* **2009**, 21, 2632.
- [109] K. Jung, H. Seo, Y. Kim, H. Im, J. Hong, J.-W. Park, J.-K. Lee, *Appl. Phys. Lett.* **2007**, 90, 052104.
- [110] K. Terabe, T. Hasegawa, T. Nakayama, M. Aono, *Nature* **2005**, 433, 47.
- [111] S. Gao, F. Zeng, C. Chen, G. Tang, Y. Lin, Z. Zheng, C. Song, F. Pan, *Nanotechnology* **2013**, 24, 335201.
- [112] A. Younis, D. Chu, S. Li, *Sci. Rep.* **2015**, 5, 13599.
- [113] I. Valov, *Semicond. Sci. Technol.* **2017**, 32, 093006.
- [114] E. W. Lim, R. Ismail, *Electronics* **2015**, 4, 586.
- [115] S. Kim, S. Jung, M. H. Kim, S. Cho, B. G. Park, *Appl. Phys. Lett.* **2015**, 106, 212106.
- [116] M. J. Lee, C. B. Lee, D. Lee, S. R. Lee, K. Kim, *Nat. Mater.* **2011**, 10, 625.
- [117] K. Nagashima, T. Yanagida, K. Oka, M. Taniguchi, T. Kawai, J. S. Kim, B. H. Park, *Nano Lett.* **2010**, 10, 1359.
- [118] A. Younis, D. Chu, X. Lin, J. Yi, F. Dang, S. Li, *ACS Appl. Mater. Interfaces* **2013**, 5, 2249.
- [119] H. Tian, L. Zhao, X. Wang, Y. W. Yeh, N. Yao, B. P. Rand, T. L. Ren, *ACS Nano* **2017**, 11, 12247.
- [120] A. Younis, D. Chu, I. Mihail, S. Li, *ACS Appl. Mater. Interfaces* **2013**, 5, 9429.
- [121] X. Yan, J. Zhao, S. Liu, Z. Zhou, Q. Liu, J. Chen, X. Y. Liu, *Adv. Funct. Mater.* **2018**, 28, 1705320.
- [122] C. A. Santini, A. Sebastian, C. Marchiori, V. P. Jonnalagadda, L. Dellmann, W. W. Koelmans, M. D. Russell, C. P. Rossel, E. Eleftheriou, *Nat. Commun.* **2015**, 6, 8600.
- [123] Z. Zhang, Y. Wang, Y. Luo, Y. He, M. Ma, R. Yang, H. Li, *Sci. Rep.* **2018**, 8, 12617.
- [124] A. M. Rana, T. Akbar, M. Ismail, E. Ahmad, F. Hussain, I. Talib, M. Imran, K. Mehmood, K. Iqbal, M. Y. Nadeem, *Sci. Rep.* **2017**, 7, 39539.
- [125] Y. C. Chang, C. J. Lee, L. W. Wang, Y. H. Wang, *Small* **2018**, 14, 1703888.
- [126] S. Sung, C. Wu, H. S. Jung, T. W. Kim, *Sci. Rep.* **2018**, 8, 12081.
- [127] X. F. Wang, H. Tian, H. M. Zhao, T. Y. Zhang, W. Q. Mao, Y. C. Qiao, Y. Pang, Y. X. Li, Y. Yang, T. L. Ren, *Small* **2018**, 14, 1702525.
- [128] Y. H. Ting, J. Y. Chen, C. W. Huang, T. K. Huang, C. Y. Hsieh, W. W. Wu, *Small* **2018**, 14, 1703153.
- [129] X. Zhao, Z. Wang, Y. Xie, H. Xu, J. Zhu, X. Zhang, W. Liu, G. Yang, J. Ma, Y. Liu, *Small* **2018**, 14, 1801325.
- [130] X. Yan, Y. Pei, H. Chen, J. Zhao, Z. Zhou, H. Wang, L. Zhang, J. Wang, X. Li, C. Qin, G. Wang, Z. Xiao, Q. Zhao, K. Wang, H. Li, D. Ren, Q. Liu, H. Zhou, J. Chen, P. Zhou, *Adv. Funct. Mater.* **2018**, 31, 1805284.
- [131] S. Lee, J. Sohn, Z. Jiang, H. Y. Chen, H. S. P. Wong, *Nat. Commun.* **2015**, 6, 8407.
- [132] J. T. Wang, K. Saito, H. C. Wu, H. S. Sun, C. C. Hung, Y. Chen, T. Isono, T. Kakuchi, T. Satoh, W. C. Chen, *NPG Asia Mater.* **2016**, 8, e298.
- [133] X. F. Wang, H. Tian, H. M. Zhao, T. Y. Zhang, W. Q. Mao, Y. C. Qiao, Y. Pang, Y. X. Li, Y. Yang, T. L. Ren, *Small* **2018**, 14, 1702525.
- [134] C. Hao, F. Wen, J. Xiang, S. Yuan, B. Yang, L. Li, W. Wang, Z. Zeng, L. Wang, Z. Liu, Y. Tian, *Adv. Funct. Mater.* **2016**, 26, 2016.
- [135] H. Y. Jeong, J. Y. Lee, S. Y. Choi, *Adv. Funct. Mater.* **2010**, 20, 3912.
- [136] Y. Wang, Q. Liu, S. Long, W. Wang, Q. Wang, M. Zhang, *Nanotechnology* **2009**, 21, 045202.
- [137] B. Gao, H. W. Zhang, S. Yu, B. Sun, L. F. Liu, X. Y. Liu, Y. Wang, R. Q. Han, J. F. Kang, B. Yu, Y. Y. Wang, In *2009 Symp. on VLSI Technology*, IEEE, Piscataway, NJ **2009**, pp. 30–31.
- [138] Z. Wang, W. G. Zhu, A. Y. Du, L. Wu, Z. Fang, X. A. Tran, W. J. Liu, K. L. Zhang, H. Y. Yu, *IEEE Trans. Electron. Dev.* **2012**, 59, 1203.
- [139] Y. B. Kim, S. R. Lee, D. Lee, C. B. Lee, M. Chang, J. H. Hur, J. H. Hur, M. J. Lee, G. S. Park, C. J. Kim, U. I. Chung, I. K. Yoo, K. Kim, In *VLSI Technology (VLSIT)*, 2011 Symp. On, IEEE, Piscataway, NJ (pp. 52–53).
- [140] H. Zhang, L. Liu, B. Gao, Y. Qiu, X. Liu, J. Lu, R. Han, J. Kang, B. Yu, *Appl. Phys. Lett.* **2011**, 98, 042105.
- [141] E. J. Yoo, M. Lyu, J. H. Yun, C. J. Kang, Y. J. Choi, L. Wang, *Adv. Mater.* **2005**, 27, 6170.
- [142] J. Yao, J. Lin, Y. Dai, G. Ruan, Z. Yan, L. Li, L. Zhong, D. Natelson, J. M. Tour, *Nat. Commun.* **2012**, 3, 1101.
- [143] X. Yan, J. Wang, M. Zhao, X. Li, H. Wang, L. Zhang, C. Lu, D. Ren, *Appl. Phys. Lett.* **2018**, 113, 013503.
- [144] S. Tanachutiwat, M. Liu, W. Wang, *IEEE Trans. VLSI Syst.* **2011**, 19, 2023.
- [145] K. K. Likharev, *J. Nanoelectron. Optoelectron.* **2008**, 3, 203.
- [146] D. B. Strukov, G. S. Snider, D. R. Stewart, R. S. Williams, *Nature* **2008**, 453, 80.
- [147] Y. He, Y. Yang, S. Nie, R. Liu, Q. Wan, *J. Mater. Chem. C* **2018**, 6, 5336.
- [148] J. S. Najem, G. J. Taylor, R. J. Weiss, M. S. Hasan, G. Rose, C. D. Schuman, A. Belianinov, C. P. Collier, S. A. Sarles, *ACS Nano* **2018**, 12, 4702.
- [149] P. M. Sheridan, F. Cai, C. Du, W. Ma, Z. Zhang, W. D. Lu, *Nat. Nanotechnol.* **2017**, 12, 784.
- [150] C. S. Yang, D. S. Shang, N. Liu, E. J. Fuller, S. Agrawal, A. A. Talin, Y. Q. Li, B. G. Shen, Y. Sun, *Adv. Funct. Mater.* **2018**, 28, 1804170.
- [151] N. Raghavan, D. D. Frey, M. Bosman, K. L. Pey, In *IEEE International Reliability Physics Symposium*, IEEE, Piscataway, NJ **2015** (p. 5).
- [152] H. Xie, Q. Liu, Y. Li, H. Lv, M. Wang, X. Liu, H. Sun, X. Yang, S. Long, S. Liu, M. Liu, *Semiconductorence Technol.* **2012**, 27, 125008.
- [153] Z. Fang, H. Y. Yu, X. Li, N. Singh, G. Q. Lo, D. L. Kwong, *IEEE Electron. Device Lett.* **2011**, 32, 566.
- [154] W. Banerjee, N. Lu, Y. Yang, L. Li, H. Lv, Q. Liu, S. Long, M. Liu, *IEEE Trans. Electron Devices* **2018**, 99, 1.
- [155] S. Yu, H. Y. Chen, Y. Deng, B. Gao, Z. Jiang, J. Kang, H. S. P. Wong, In *VLSIT, 2013 Symp. On*, IEEE, Piscataway, NJ (pp. T158–T159).
- [156] H. Y. Chen, S. Brivio, C. C. Chang, J. Frascaroli, T. H. Hou, B. Hudec, M. Liu, H. Lv, G. Molas, J. Sohn, S. Spiga, V. M. Teja, E. Vianello, H. S. P. Wong, *J. Electroceram.* **2017**, 39, 21.